Reconstructing large scales at cosmic dawn

Selim C. Hotinli[1] and Matthew C. Johnson[2,3]
[1]*Department of Physics, Imperial College London, Blackett Laboratory, Prince Consort Road, London SW7 2AZ, United Kingdom*
[2]*Perimeter Institute for Theoretical Physics, 31 Caroline Street North, Waterloo, Ontario N2L 2Y5, Canada*
[3]*Department of Physics and Astronomy, York University, Toronto, Ontario M3J 1P3, Canada*

(Received 22 February 2021; accepted 3 March 2022; published 18 March 2022)

The cosmic microwave background (CMB) serves as a backlight to large-scale structure during the epoch of reionization, where Thomson scattering gives rise to temperature anisotropies on small angular scales from the kinetic Sunyaev Zel'dovich (kSZ) effect. In this paper, we demonstrate that the technique of kSZ tomography (velocity reconstruction), based on cross-correlations between CMB temperature and 21-cm surveys, can significantly improve constraints on models of inhomogeneous reionization and provide information about large-scale modes that are poorly characterized by 21-cm measurements themselves due to foreground contamination.

DOI: 10.1103/PhysRevD.105.063522

I. INTRODUCTION

The epoch of reionization (EOR), corresponding to the time when the first stars formed (cosmic dawn) and ionized the majority of neutral hydrogen in the Universe, is among the least understood parts of our cosmic history. Excitingly, surveys of the redshifted 21-cm hydrogen line such as HERA [1] and SKA [2], cosmic microwave background (CMB) experiments such as the Simons Observatory (SO) [3], CMB-S4 [4] and CMB-HD [5,6], as well as infrared, x-ray, and line intensity mapping missions promise to deliver an abundance of information on the EOR in the coming decade. There is much to learn about astrophysics from EOR measurements. Additionally, because it is a high redshift probe, the EOR in principle carries information about cosmology. In this paper, we propose a new method for extracting both astrophysical and cosmological information from the EOR by combining data from 21-cm and CMB surveys using the technique of kinetic Sunyaev Zel'dovich (kSZ) tomography [7–10].

A few hundred million years after the big bang, the Universe went through a phase of patchy reionization, where local bubbles of ionized gas formed around the first stars initiated, and eventually completed, the transition to a fully ionized baryonic component of the Universe. As patchy reionization unfolds, CMB photons Thompson scatter from free electrons inside the bubbles, giving rise to temperature anisotropies proportional to the local density and the CMB dipole observed in the rest frame of the electrons [11–14]. This is the kSZ effect [15–18], referred to here as "reionization kSZ" to distinguish the present context from lower redshift contributions to the kSZ temperature anisotropies. Reionization kSZ makes an important blackbody contribution to the observed CMB temperature anisotropies on small angular scales, and with detection imminent in the next generation CMB experiments, there have been significant recent efforts to model reionization kSZ with increasing accuracy (see e.g., Refs. [19,20]) and devise statistics to extract information about reionization (see e.g., Refs. [21–23]).

Given a tracer of the ionized bubbles formed during patchy reionization, we show that it is possible to extract information about the remote dipole field (the projected CMB dipole observed along our past light cone; see e.g., Refs. [9,24]) from the measured reionization kSZ temperature anisotropies. We develop a quadratic estimator [9,10] for the dipole field based on the correlations between the redshifted 21-cm hydrogen line, which is anticorrelated with ionized regions [25,26], and CMB temperature anisotropies on small angular scales. Because reionization occurs at relatively high redshifts ($z \sim 7.5$, corresponding to a radial comoving distance of $\sim$9 Gpc), the remote dipole field contains information about inhomogeneities on very large physical scales, making it a useful cosmological probe. Indeed, direct measurements of 21 cm on large scales can improve constraints on e.g., the optical depth [27], ΛCDM [28], neutrino masses [29], isocurvature [30], or the running of the spectral index [31]. However, using 21 cm on large scales to infer the underlying density field will be difficult due to foreground contamination [32], making the information in the reconstructed dipole field highly valuable and entirely complementary to direct 21-cm observations.

Cross-correlations between 21 cm and kSZ also provide constraints on models of reionization. Previous literature

has considered constraints deriving from the kSZ–21-cm cross power [33–37] as well as higher-order statistics such as the kSZ–kSZ–21-cm bispectrum [38,39]. In this paper, we propose that correlations between the remote dipole field and 21-cm observations can provide tight constraints on models of reionization. This is equivalent to the 21-cm–21-cm–kSZ bispectrum, in complete analogy with recent results on the late-time kSZ effect [10], which in the context of reionization was shown in Ref. [25] to contain more information than the kSZ–21-cm cross power. Another probe of reionization comes from small-angular scale measurements of CMB polarization, which can be used to reconstruct the inhomogeneous optical depth during reionization [40]. We show that including correlations between the reconstructed optical depth, 21 cm, and the remote dipole field improves constraints due to complementary parameter degeneracies.

II. OBSERVABLES

Including fluctuations in the ionization fraction along a line of sight $\hat{\mathbf{n}}$ at a radial comoving distance χ, the optical depth is defined as

$$\tau(\chi\hat{\mathbf{n}}) = -\sigma_T \int d\chi a(\chi)\bar{n}_b(\chi)[\bar{x}_e(\chi) + \delta x_e(\chi\hat{\mathbf{n}})]. \quad (1)$$

In terms of redshift z, we define the mean ionization fraction during reionization as

$$\bar{x}_e(z) = \frac{1}{2}\left[1 - \tanh\left(\frac{y(z) - y_{\rm re}}{\Delta_y}\right)\right], \quad (2)$$

where Δ_y and $y_{\rm re}$ are model parameters and $y(z) = (1+z)^{3/2}$. We trade $y_{\rm re}$ for the mean optical depth

$$\tau = -\sigma_T \int d\chi a(\chi)\bar{n}_b(\chi)\bar{x}_e(\chi). \quad (3)$$

We model the inhomogeneities in the ionization fraction following Refs. [40–42] as due to bubbles[1] whose radius R follows a log-normal distribution with mean size $\bar{R}$ and width $\sigma_{\ln R}$

$$P(R) = R^{-1}(2\pi^2\sigma_{\ln R}^2)^{-0.5}\exp\{-\ln[(R/\bar{R})^2]/(2\sigma_{\ln R}^2)\}. \quad (4)$$

[1]The bubble model is an analytic approximation of the reionization physics and may not represent the Universe sufficiently accurately compared to more realistic reionization simulations. Our goal here is to demonstrate the potential benefit of velocity tomography during reionization without going into further detail about complicated and less known astrophysics including baryonic feedback effects, for example. Later in our forecasts, we will introduce and marginalize over a bias parameter to capture the effects that might drive the signal away from the bubble-model prediction in reality.

Finally, we assume the number density of bubbles fluctuates as a biased tracer of the large-scale structure with a bubble bias b. We set the fiducial values of our reionization model as $\{\tau, \Delta_y, b, \bar{R}, \sigma_{\ln R}\} = \{0.06, 7.0, 6.0, 5\ \text{Mpc}, 0.7\}$. Note that we translate the constraints on Δ_y into another common parametrization, $\Delta z = z|_{\bar{x}_e=0.75} - z|_{\bar{x}_e=0.25}$, with fiducial value $\Delta z_0 = 1.66$ for our parameter choices.

A. Hydrogen power spectra

Surveys of 21-cm hydrogen line measure the brightness temperature. We model the amplitude of the brightness temperature fluctuation, $\delta T_{21}(\chi\hat{\mathbf{n}}) \equiv \bar{T}_{21}(\chi) - T_{21}(\chi\hat{\mathbf{n}})$, as proportional to the neutral hydrogen density fluctuation, $\delta T_{21}(\chi\hat{\mathbf{n}}) = F^{1/2}(\chi)\delta_{\rm H}(\chi\hat{\mathbf{n}})$, where in terms of redshift

$$F^{1/2}(z) = 0.023\ \text{K}\frac{1-Y_p}{0.75}\frac{\Omega_b h^2}{0.02}\left(\frac{1+z}{10}\frac{0.15}{\Omega_m h^2}\right) \quad (5)$$

and Y_p is the primordial helium fraction. Note we ignored modeling complicating factors such as the baryonic feedback, spatial fluctuations in spin temperature and the effect of redshift-space distortions, which are beyond the scope of our paper. We account for these astrophysical uncertainties by marginalizing over the amplitude of the 21-cm hydrogen spectra when forecasting.

The neutral hydrogen fluctuations can be separated into contributions from the ionization fraction and the gas density function $\delta(\chi\hat{\mathbf{n}})$, as e.g., in [41,43,44]:

$$\delta_{\rm H}(\chi\hat{\mathbf{n}}) = [1 - \bar{x}_e(\chi\hat{\mathbf{n}})]\delta(\chi\hat{\mathbf{n}}) - \delta x_e(\chi\hat{\mathbf{n}}). \quad (6)$$

Ionized hydrogen fluctuations, or equivalently the free electron, satisfy $\delta_e(\chi\hat{\mathbf{n}}) = \bar{x}_e\delta(\chi\hat{\mathbf{n}}) + \delta x_e(\chi\hat{\mathbf{n}})$.

Following [41,43,44], we work in the context of the halo model [45] and express power spectra in terms of correlations between (two-bubble) and within (one-bubble) reionization bubbles. For the forecasts presented below, we need the power spectra for hydrogen $P_{\rm HH}(k,z) = \langle\delta_{\rm H}(k,z)^2\rangle$, electrons $P_{ee}(k,z) = \langle\delta_e(k,z)^2\rangle$, and cross powers, $P_{e\rm H}$ and $P_{\delta\rm H}$. The large-scale two-bubble hydrogen-intensity and electron power spectra are

$$P_{\rm HH}^{2b} = [(1-\bar{x}_e)(\ln(1-\bar{x}_e)b\langle W_R(k)\rangle + 1)]^2 P_{\delta\delta}(k), \quad (7)$$

$$P_{ee}^{2b}(z) = [(1-\bar{x}_e)\ln(1-\bar{x}_e)b\langle W_R(k)\rangle - \bar{x}_e]^2 P_{\delta\delta}(k), \quad (8)$$

where $P_{\delta\delta}(k)$ is the linear matter power spectrum,

$$\langle W_R(k)\rangle = \langle V_b\rangle^{-1}\int {\rm d}R P(R) V_b(R) W_R(k), \quad (9)$$

where mean bubble volume is $\langle V_b\rangle \equiv \int {\rm d}R P(R) V_b(R)$, and

$$W_R(k) \equiv 3(kR)^{-1}[\sin(kR) - kR\cos(kR)]. \quad (10)$$

Note we omit showing redshift dependence of the ionization fraction and the power spectra for notational brevity. Following [44], the small-scale one-bubble power spectra are

$$P^{1b}_{\rm HH} = P^{1b}_{ee} \simeq \bar{x}_e(1-\bar{x}_e)[\langle V_b\rangle\langle W_R^2(k)\rangle + \tilde{P}(k)], \quad (11)$$

where $\langle W_R^2(k)\rangle \equiv \langle V_b\rangle^{-2}\int {\rm d}R V_b^2(R)P(R)W_R^2(k)$,

$$\tilde{P}(k) \simeq P(k)\langle V_b\rangle\langle\sigma_R^2\rangle[P(k)^2 + (\langle V_b\rangle\langle\sigma_R^2\rangle)^2]^{-1/2}, \quad (12)$$

and $\langle\sigma_R^2\rangle$ is the smoothed density variance averaged over the bubble radius distribution:

$$\langle\sigma_R^2\rangle = \langle V_b\rangle^{-2}\int {\rm d}R V_b^2(R)P(R)\sigma_R^2. \quad (13)$$

Finally, the cross-correlations between the matter density, the neutral hydrogen and the free electron fluctuations can be found as $P^{2b}_{\rm eH}(k) = P_{{\rm H}\delta}(k) - P^{2b}_{\rm HH}(k)$, where

$$P_{{\rm H}\delta}(k) = (1-\bar{x}_e)[\ln(1-\bar{x}_e)b\langle W_R(k)\rangle - 1]P_{\delta\delta}(k) \quad (14)$$

and $P^{1b}_{\rm eH}(k) = -P^{1b}_{\rm ee}(k)$.

B. Temperature and polarization anisotropies

Temperature anisotropies in the $\hat{\mathbf{n}}$ direction are sourced during reionization by the kSZ effect and the screening of the primary CMB temperature anisotropies $\Theta_p(\hat{\mathbf{n}})$ [40,46]:

$$\Theta_{\rm rei}(\hat{\mathbf{n}}) \simeq \int_{\rm rei} {\rm d}\chi\dot{\tau}(\chi\hat{\mathbf{n}})e^{-\tau(\chi)}[v_{\rm eff}(\chi\hat{\mathbf{n}}) - \Theta_p(\hat{\mathbf{n}})] \quad (15)$$

$$\simeq \sum_\alpha [\bar{v}^\alpha_{\rm eff}(\hat{\mathbf{n}}) - \Theta_p(\hat{\mathbf{n}})]\int_{\chi^\alpha_{\rm min}}^{\chi^\alpha_{\rm max}} {\rm d}\chi\dot{\tau}(\chi\hat{\mathbf{n}})e^{-\tau(\chi)} \quad (16)$$

$$\simeq \sum_\alpha [\bar{v}^\alpha_{\rm eff}(\hat{\mathbf{n}}) - \Theta_p(\hat{\mathbf{n}})]\Delta\tau^\alpha(\hat{\mathbf{n}}), \quad (17)$$

where the optical depth and its χ derivative $\dot{\tau}$ are defined by Eq. (1) and $v_{\rm eff} = 3\int {\rm d}^2\hat{\mathbf{n}}_e\Theta_1(\chi\hat{\mathbf{n}},\hat{\mathbf{n}}_e)\hat{\mathbf{n}}\cdot\hat{\mathbf{n}}_e/(4\pi)$ is the remote dipole field projected along the line of sight; note that we neglect the evolution of the primary CMB between reionization and the present day (e.g., due to the integrated Sachs-Wolfe effect). In the second line, we bin the contribution to the visibility, approximate the remote dipole by its bin average, and neglect terms beyond linear order in τ. Note that while the dominant contribution to the remote dipole field is the Doppler effect due to local peculiar velocity, there is a significant primordial contribution from the Sachs Wolfe effect on the largest angular scales. We contrast the full and Doppler contribution to the remote dipole power spectrum in Fig. 1; we also show the primary CMB temperature fluctuations for reference.

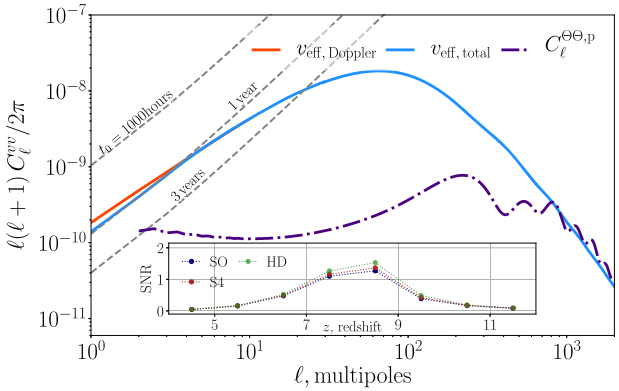

FIG. 1. Dipole field in a redshift bin centered at $z = 8.5$ and of size $\Delta z = 1$ (blue solid line), shown with its Doppler component (orange solid line) and the primary CMB (purple dot-dashed line). Dashed gray lines show reconstruction noise forecasts from the combination of CMB S4 and SKA survey, latter for varying integration times $t_0 = \{1000\ {\rm h}, 1\ {\rm yr}, 3\ {\rm yr}\}$ from top to bottom. The inset plot shows the SNR forecasts per redshift bins of size $\Delta z = 1$, for varying CMB experiments and 1000 h of measurement time for a SKA-like experiment.

Analogously, the polarization anisotropies during reionization are sourced by Thomson, the polarized Sunyaev Zel'dovich (pSZ) effect, and screening of polarization anisotropies produced at recombination. The contributions due to inhomogeneous reionization are

$$\Theta^\pm_{\rm rei}(\hat{\mathbf{n}}) \simeq \sum_\alpha [\bar{q}^{\pm;\alpha}_{\rm eff}(\hat{\mathbf{n}}) - \Theta^\pm_{\rm rec}(\hat{\mathbf{n}})]\Delta\tau^\alpha(\hat{\mathbf{n}}), \quad (18)$$

where $\Theta^\pm \equiv (Q \pm iU)$ and $\bar{q}^{\pm;\alpha}_{\rm eff}(\hat{\mathbf{n}})$ is the bin-averaged remote quadrupole field (the locally observed CMB quadrupole).

III. RECONSTRUCTION

The temperature and polarization anisotropies sourced during patchy reionization from a redshift bin are products of the anisotropic optical depth $\Delta\tau^\alpha(\hat{\mathbf{n}})$ and the difference of the dipole or quadrupole fields and primordial temperature or polarization anisotropies. Given the dipole or quadrupole fields and the temperature or polarization anisotropies, Ref. [40] constructed a quadratic estimator for the anisotropic optical depth $\Delta\tau(\hat{\mathbf{n}}) \equiv \sum_\alpha \Delta\tau^\alpha(\hat{\mathbf{n}})$ (in fact, a weighted sum is reconstructed; we neglect this complication for the moment). Turning this around, Ref. [47] constructed a quadratic estimator for the polarization anisotropies given a tracer of the anisotropic optical depth.

In this paper, we propose a new quadratic estimator for the remote dipole field using the 21-cm line as a (redshift-dependent) tracer of the anisotropic optical depth. In

analogy with the estimator for the late-time kSZ effect [9], the estimator for the averaged remote dipole field over redshift bin α is

$$\hat{v}^{\alpha}_{\mathrm{eff},\ell m} = b_v^{\alpha} N^{vv}_{\alpha\ell} \sum_{\ell_1 m_1 \ell_2 m_2} (-1)^m \Gamma^{\alpha}_{\ell_1\ell_2\ell} \begin{pmatrix} \ell_1 & \ell_2 & \ell \\ m_1 & m_2 & -m \end{pmatrix} \times \frac{a^{\Theta}_{\ell_1 m_1} \delta^{\alpha}_{H,\ell_2 m_2}}{C^{\Theta\Theta,\mathrm{obs}}_{\ell_1} C^{\mathrm{HH,obs}}_{\alpha\ell_2}}, \tag{19}$$

where b_v^{α} is the "optical depth bias," which, in our study, is due to mismodeling $C^{\tau\mathrm{H}}_{\alpha,\ell_2}$ in the presence of foregrounds, baryonic feedback and other factors that bias the relation between the observed temperature brightness and the hydrogen density, $\delta T_{21} \to b_H F^{1/2}(z)\delta_{\mathrm{H}}(\chi\hat{\mathbf{n}})$, and the optical depth bias is a function of b_{H} whose functional form is shown in Eq. (69) of Ref. [10]. The coefficient is

$$\Gamma^{\alpha}_{\ell_1\ell_2\ell} = \sqrt{\frac{(2\ell_1+1)(2\ell_2+1)(2\ell+1)}{4\pi}} \begin{pmatrix} \ell_1 & \ell_2 & \ell \\ 0 & 0 & 0 \end{pmatrix} C^{\tau\mathrm{H}}_{\alpha,\ell_2}, \tag{20}$$

and the reconstruction noise (i.e., variance of the estimator) is defined by

$$\frac{1}{N^{vv}_{\alpha\ell}} = \frac{1}{(2\ell+1)} \sum_{\ell_1\ell_2} \frac{\Gamma^{\alpha}_{\ell_1\ell_2\ell}\Gamma^{\alpha}_{\ell_1\ell_2\ell}}{C^{\Theta\Theta,\mathrm{obs}}_{\ell_1} C^{\mathrm{HH,obs}}_{\alpha\ell_2}}. \tag{21}$$

In these expressions, $C^{\Theta\Theta,\mathrm{obs}}_{\ell_1}$ is the measured CMB temperature power spectrum, $C^{\mathrm{HH,obs}}_{\alpha\ell_2}$ is the measured spectrum of the mean 21-cm hydrogen fluctuations in each redshift bin, $\delta^{\mathrm{obs}}_{\mathrm{H},\alpha}(\chi\hat{\mathbf{n}}) = \int_{\chi^{\alpha}_{\mathrm{min}}}^{\chi^{\alpha}_{\mathrm{max}}} \mathrm{d}\chi W_{\alpha}(\chi)\delta^{\mathrm{obs}}_{\mathrm{H}}(\chi\hat{\mathbf{n}})$, where $W_{\alpha}(\chi)$ is a top-hat selection function for redshift bin α, and $C^{\tau\mathrm{H}}_{\alpha,\ell_2}$ is the cross power of the optical depth and brightness temperature counts in each bin.

In principle, the reconstruction noise improves by probing increasing small angular scales with the CMB and brightness temperature and is limited only by the vanishing τ and H correlation on very small scales. In reality, the reconstruction noise is limited by the instrumental noise of the CMB experiment and thermal noise of the 21-cm experiment, since this places an effective upper limit in ℓ on the sum in Eq. (21). Due to the contribution from screening, the reconstruction in each bin will be biased by $\Theta_p(\hat{\mathbf{n}})$; this can be subtracted using our knowledge of the well-measured primary CMB on large angular scales.

Below, we also make use of the reconstructed anisotropic optical depth from measurements of CMB polarization. The quadratic estimator for $\Delta\tau(\hat{\mathbf{n}})$ was given in Ref. [40]; the variance is

$$N^{\tau\tau}_{\ell} = \left[\frac{1}{2\ell+1} \sum_{\ell_1\ell_2} \frac{|\Gamma^{\mathrm{EB}}_{\ell_1\ell_2\ell}|^2}{(C^{\mathrm{EE}}_{\ell_1} + N^{\mathrm{EE}}_{\ell_1})(C^{\mathrm{BB}}_{\ell_2} + N^{\mathrm{BB}}_{\ell_2})}\right]^{-1}, \tag{22}$$

with

$$\Gamma^{\mathrm{EB}}_{\ell_1\ell_2\ell} = \frac{C^{E_0E_1}_{\ell_1}}{2i} \sqrt{\frac{(2\ell_1+)(2\ell_2+1)(2\ell+1)}{4\pi}} \times \left[\begin{pmatrix} \ell_1 & \ell_2 & \ell \\ -2 & 2 & 0 \end{pmatrix} - \begin{pmatrix} \ell_1 & \ell_2 & \ell \\ 2 & -2 & 0 \end{pmatrix}\right], \tag{23}$$

where $C^{E_0E_1}_{\ell_1}$ is the cross power between the E-mode polarization anisotropies with (E_1) and without (E_0) the contributions from patchy reionization.

IV. FORECASTS

We model the experimental noise from the 21-cm brightness measurement as in [48], with experimental specifications appropriate to the upcoming SKA survey [49]. We apply a cutoff for the parallel Fourier modes to approximate the effect of catastrophic foregrounds, excluding modes with $k_{\parallel} < 0.01\ h/\mathrm{Mpc}$.[2] We find the SNR depends on the large-scale $k_{\parallel}$ cutoff with $\propto k^{-2}_{\mathrm{cut}}$. We ignore the so-called foreground wedge (see e.g., Ref. [32]) that limits the observation of the small-scale transverse modes in combination with the large-scale radial modes, since, in principle, foregrounds do not lead to a loss of information (a similar approach is taken in e.g., [50]), and the wedge can potentially be removed with better understanding of the instrument [51,52].

We divide the 21-cm survey into eight redshift bins inside the range $z \in [4, 12]$.[3] For a total integration time of 1000 h for the 21-cm experiment, the total detection SNR (assuming zero null condition in the reconstructed dipole field) is $\{3.0, 3.2, 3.4\}$ for SO, CMB-S4 and CMB-HD, respectively. We show the detection SNR per redshift bin in the inset of Fig. 1. We find, for a full 3-yr 21-cm experiment, the SNR can reach $\{15.6, 16.3, 17.5\}$ for the same set of experiments. We find that in all cases the 21-cm experimental noise dominates the kSZ reconstruction error.

With an SKA-like experiment, it is possible to produce maps of the dipole field over a significant range of scales. This is illustrated by Fig. 1, which compares the remote dipole power spectrum to the reconstruction noise in a

[2]The parameter constraints we show later in this section depend marginally on this large-scale $k_{\parallel}$ cutoff, as they are more significantly determined by the cross-correlation between the reconstructed velocity field and the hydrogen on smaller scales $k_{\parallel} \gtrsim 0.03\ h/\mathrm{Mpc}$. The large-scale $k_{\parallel}$ cutoff is more detrimental to the SNR (shown in the inset of Fig. 1) measured from the kSZ tomography in cross-correlation with the 21-cm signal.

[3]We find dividing the redshift range into narrower redshift bins does not improve the total SNR for the experimental specifications we consider in this paper.

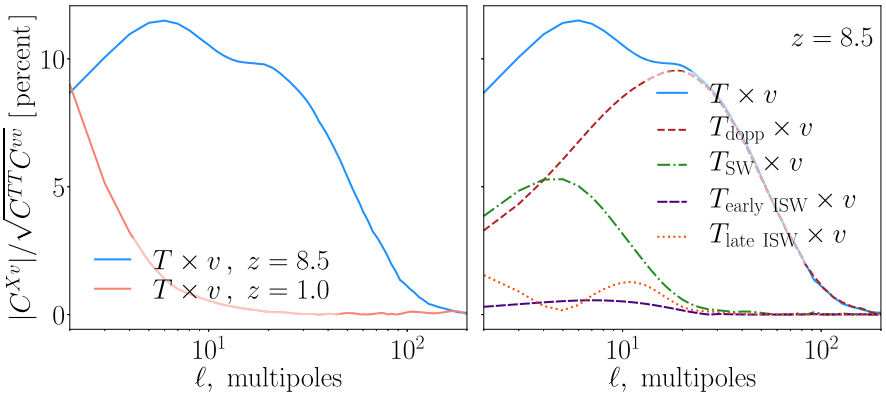

FIG. 2. Left: correlation coefficient $|C^{Xv}|/\sqrt{C^{\rm TT}C^{vv}}$ between the CMB temperature and the remote dipole at two redshifts $z \in \{1.0, 8.5\}$. For higher redshifts remote dipole probes CMB at higher accuracy and precision. Right: correlation coefficient between varying contributions to the CMB temperature $X \in \{T_{\rm dopp}, T_{\rm SW}, T_{\rm ISW}\}$ and the remote dipole. The larger range of ℓ, accessible to higher redshifts, allows probing different components of the CMB at different scales.

redshift bin centered at $z = 8.5$. The cosmological value of the dipole field reconstructed at lower redshift has been established in many recent studies [24,53–58]. Maps of the remote dipole field at reionization probe larger scales, which we illustrate by computing the correlation coefficient between the dipole field at a variety of redshifts and the primary CMB, as shown in Fig. 2. During reionization, there is correlation at the ∼10% level with a variety of the contributions to the primary CMB over a significant range of multipoles. We can therefore conclude that the remote dipole field contains new information on scales comparable to the primary CMB, making it a promising observable to improve upon cosmic-variance limited constraints from the primary CMB alone. Furthermore, the correlation structure between the remote dipole field and the various components of the CMB (right panel of Fig. 2) can potentially be used to break degeneracies suffered by other probes of cosmology and to improve constraints on parameters sensitive to large-scale CMB and density fluctuations. We leave a detailed study to future work.

Turning to potential constraints on reionization, we construct the Fisher matrix incorporating various combinations of 21 cm, the remote dipole, and the reconstructed optical depth

$$F_{ab} = \sum_{\ell=\ell_{\rm min}}^{\ell_{\rm max}} f_{\rm sky} \frac{2\ell+1}{2} {\rm Tr}[(\partial_a \mathbf{C}_\ell)\mathbf{C}_\ell^{-1}(\partial_b \mathbf{C}_\ell)\mathbf{C}_\ell^{-1}], \quad (24)$$

where indices $\{a, b\}$ represent reionization model parameters introduced earlier (we assume the standard LCDM model with cold matter and dark energy whose parameters we fix to *Planck* 2018 cosmology [59]). We assume the Fisher matrix for the optical depth reconstruction to be independent from the kSZ tomography and set the covariance matrix $\mathbf{C}_\ell$ for the latter to include autocorrelations of the neutral hydrogen and the remote dipole, as well as their correlations, between eight redshift bins. We add an additional bias parameter for the temperature brightness at every redshift bin, effectively marginalizing over both the amplitude of $\delta_{\rm H}(\chi\hat{\mathbf{n}})$ and the optical depth bias from the kSZ, which are expected to be subject to large model uncertainties.

We show our results in Fig. 3 for the anticipated noise levels from an SKA-like experiment, with 1000 h of integration time, together with the constraints from optical depth reconstruction from the CMB. We find $\sigma(\tau) \lesssim 3.0 \times 10^{-3}$ from measurement of $C_\ell^{\rm HH}$ alone, and, with a CMB-S4-like experiment, $\sigma(\tau) \lesssim 5.0 \times 10^{-3}$ from $C_\ell^{\rm vH}$ and C_ℓ^{vv} together. Combined constraints from the hydrogen and remote dipole fields satisfy $\sigma(\tau) \lesssim 2.3 \times 10^{-3}$, comparable to the cosmic-variance limit that can be achieved from large-angle CMB polarization data. The right plot in Fig. 3 suggests that the potential improvement on the reionization parameters from the kSZ reconstruction is comparable to the τ reconstruction and the measurement of hydrogen density fluctuations alone, while better modeling the baryonic feedback mechanisms can potentially increase the constraining power of the hydrogen density beyond the velocities and the τ field. Note that the spectra from reconstructed velocity fields and the anisotropic optical depth experience different degeneracy which contributes to the constraining power of combining all these measurements together, as can be seen from the left plot in Fig. 3.

V. DISCUSSION

In this work, we discussed the scientific value of the cross-correlation between the kSZ effect, which dominantly sources CMB temperature fluctuations on small scales, and the hydrogen signal from the patchy reionization. While measuring individual sources is difficult, as they can be confused with other effects, statistical combination of the signals with a common bulk motion, as we discussed here, allows recovering cosmological

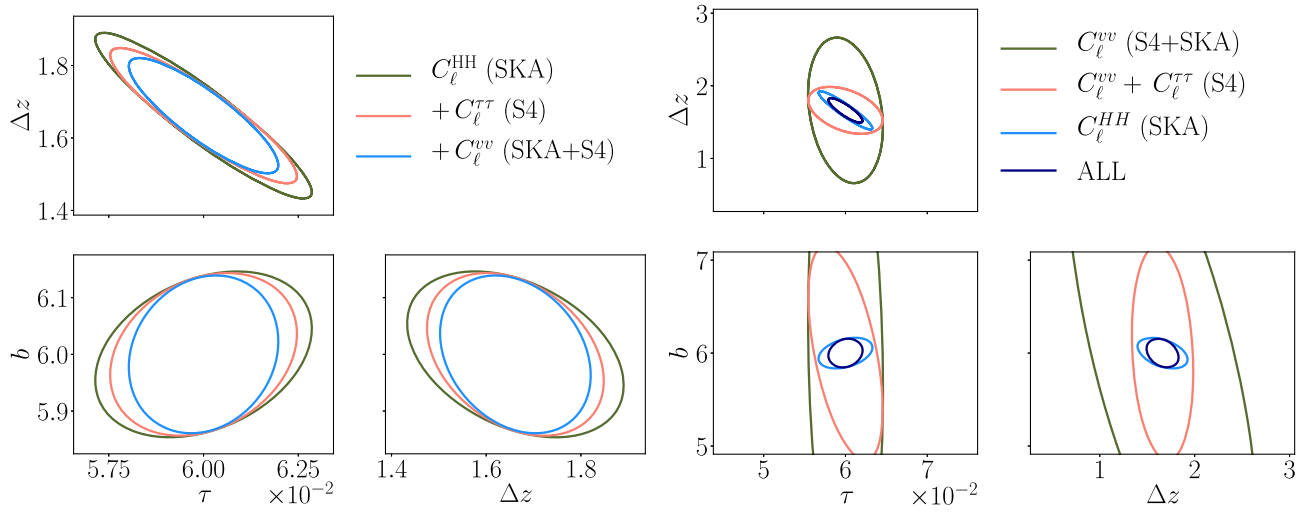

FIG. 3. Fisher forecasts on reionization parameters for 68% confidence limit from kSZ-reconstructed large-scale velocity fluctuations, reconstructed anisotropic τ field, and the neutral hydrogen fluctuations on large scales, $\ell < 300$. For the velocity reconstruction, we use eight redshift bins in the range $z \in [4, 12]$. The 21-cm experiment specifications are chosen similar to that of SKA, with 40% mutual sky coverage with the CMB experiment. The SKA measurements assume 1000 h of observation time. Left: the improvement in the astrophysical parameter constraints from addition of reconstructed $C_\ell^{\tau\tau}$ and C_ℓ^{vv} to the hydrogen power spectrum $C_\ell^{\rm HH}$, successively. Right: different degeneracies experienced by the reconstructed velocities alone (gray contours), together with the case of combining reconstructed anisotropic optical-depth spectrum with the reconstructed-velocity power-spectrum spectrum (salmon contours). The improvement from combination of these observables is due to different degeneracies that the reconstructed τ and v fields possess. These observable combinations provide constraints with degeneracy directions that are different than that of the hydrogen density power spectrum alone (in light blue colors). The dark blue contours correspond to combining all of the observables together.

information at large scales. The kSZ-reconstructed velocity field can potentially be used to break parameter degeneracies suffered by measurements of the brightness temperature (from 21-cm surveys) or the anisotropic optical depth, which can be reconstructed from the measurement of the CMB temperature and polarization, alone. In particular, we see parameters sensitive to time evolution of fluctuations during reionization, i.e., the bubble bias b and the duration of reionization Δz as well as the integrated mean optical depth τ, see improvement from measurement of the velocity field. Our improvements compare to similar studies of the kSZ effect from patchy reionization in the literature, such as Ref. [21], for example, where authors find $\sigma(\tau) \lesssim 3 \times 10^{-3}$ using kSZ reconstruction internal to CMB. Throughout we assume the late-time kSZ effect, which acts as a confusion on our velocity reconstruction, can be modeled and effectively removed from the CMB data by combined measurements of the upcoming CMB and large-scale structure surveys [10]. We will explore this "de-kSZing" procedure in an upcoming study. This work illustrates that future CMB and 21-cm experiments will provide new ways to test cosmological models and probe inhomogeneities on the very largest scales.

ACKNOWLEDGMENTS

S. C. H. is funded by Imperial College President's Scholarship, a Visiting Fellowship from the Perimeter Institute for Theoretical Physics, and a postdoctoral fellowship from Imperial College London. We thank Simone Ferraro, Mathew Madhavacheril, James Mertens, Julian Munõz and Neelima Sehgal for their useful comments. We thank Mathew Madhavacheril for providing us with realistic foreground-cleaned CMB noise estimates. We thank Juan Cayuso for providing us with precise calculation of the radial velocity spectra. Research at Perimeter Institute is supported by the Government of Canada through Industry Canada and by the Province of Ontario through the Ministry of Research and Innovation. M. C. J. was supported by the National Science and Engineering Research Council through a Discovery grant.

APPENDIX: 21-CM NOISE CALCULATION

Following Ref. [48] we define the power spectrum of system noise as

$$P_N(\mathbf{k}, z) = T_{\rm sys}(z)^2 \chi(z)^2 \lambda(z) \frac{1+z}{H(z)} \left(\frac{\lambda(z)^2}{A_e}\right)^2 \times \left(\frac{1}{N_{\rm pol} t_{\rm survey} n_b(u)}\right) \left(\frac{S_{\rm area}}{\rm FOV(z)}\right), \quad \text{(A1)}$$

where $\lambda(z) = \lambda_0(1+z)$ is the observing wavelength at redshift z, $\lambda_0 \approx 21$ cm is the transition rest-frame frequency, $S_{\rm area} = 4\pi f_{\rm sky}$ is the total survey area, $N_{\rm pol} = 2$ is the number of polarizations and $n_b(u)$ is the baseline number

density in the uv plane where $u = k_\perp \chi/(2pi)$. Here $k_\perp$ is the transverse wave number, the uv-plane density satisfies $n_b(u) = \lambda^2 n_b^{\rm phys}(\ell_a = u\lambda)$, where $n_b^{\rm phys}$ is the number of baselines as a function of physical distance of antennas as defined in Eq. (D7) of Ref. [48], and we choose hexagonal baseline arrangement as defined in Ref. [48]. We define the effective collective area as $A_e = \pi(D_{\rm eff}/2)^2$ and the effective field of view as FOV $= (\lambda/D_{\rm eff})^2$ where effective dish area is defined as $D_{\rm eff}^2 = 0.7 D_{\rm phys}^2$ [48] with $D_{\rm phys}$ is the physical dish area set to $\approx$1256.6 m^2 [2,60].

[1] D. R. DeBoer *et al.*, Publ. Astron. Soc. Pac. **129**, 045001 (2017).
[2] D. J. Bacon *et al.* (SKA Collaboration), Pub. Astron. Soc. Aust. **37**, e007 (2020).
[3] J. Aguirre *et al.* (Simons Observatory), J. Cosmol. Astropart. Phys. 02 (2019) 056.
[4] K. N. Abazajian *et al.* (CMB-S4 Collaboration), arXiv:1610.02743.
[5] N. Sehgal *et al.*, arXiv:1906.10134.
[6] N. Sehgal *et al.*, arXiv:2002.12714.
[7] P. Zhang, Mon. Not. R. Astron. Soc. **407**, L36 (2010).
[8] A. Terrana, M.-J. Harris, and M. C. Johnson, J. Cosmol. Astropart. Phys. 02 (2017) 040.
[9] A.-S. Deutsch, E. Dimastrogiovanni, M. C. Johnson, M. Münchmeyer, and A. Terrana, Phys. Rev. D **98**, 123501 (2018).
[10] K. M. Smith, M. S. Madhavacheril, M. Münchmeyer, S. Ferraro, U. Giri, and M. C. Johnson, arXiv:1810.13423.
[11] P. Valageas, A. Balbi, and J. Silk, Astron. Astrophys. **367**, 1 (2001).
[12] P.-J. Zhang, U.-L. Pen, and H. Trac, Mon. Not. R. Astron. Soc. **347**, 1224 (2004).
[13] M. McQuinn, S. R. Furlanetto, L. Hernquist, O. Zahn, and M. Zaldarriaga, Astrophys. J. **630**, 643 (2005).
[14] I. T. Iliev, U.-L. Pen, J. Bond, G. Mellema, and P. R. Shapiro, Astrophys. J. **660**, 933 (2007).
[15] Ya. B. Zeldovich, V. G. Kurt, and R. A. Sunyaev, Zh. Eksp. Teor. Fiz. **55**, 278 (1968) [Sov. Phys. JETP **28**, 146 (1969)], https://ui.adsabs.harvard.edu/abs/1969JETP...28..146Z/abstract.
[16] R. A. Sunyaev and Ya. B. Zeldovich, Astrophys. Space Sci. **7**, 20 (1970).
[17] R. A. Sunyaev and Ya. B. Zeldovich, Annu. Rev. Astron. Astrophys. **18**, 537 (1980).
[18] J. P. Ostriker and E. T. Vishniac, Astrophys. J. Lett. **306**, L51 (1986).
[19] M. A. Alvarez, Astrophys. J. **824**, 118 (2016).
[20] H. Park, M. A. Alvarez, and J. R. Bond, Astrophys. J. **853**, 121 (2018).
[21] M. A. Alvarez, S. Ferraro, J. C. Hill, R. Hložek, and M. Ikape, Phys. Rev. D **103**, 063518 (2021).
[22] K. M. Smith and S. Ferraro, Phys. Rev. Lett. **119**, 021301 (2017).
[23] S. Ferraro and K. M. Smith, Phys. Rev. D **98**, 123519 (2018).
[24] P. Zhang and M. C. Johnson, J. Cosmol. Astropart. Phys. 06 (2015) 046.
[25] A. Cooray, Phys. Rev. D **70**, 063509 (2004).
[26] R. Salvaterra, B. Ciardi, A. Ferrara, and C. Baccigalupi, Mon. Not. R. Astron. Soc. **360**, 1063 (2005).
[27] A. Liu, J. R. Pritchard, R. Allison, A. R. Parsons, U. Seljak, and B. D. Sherwin, Phys. Rev. D **93**, 043013 (2016).
[28] M. McQuinn, O. Zahn, M. Zaldarriaga, L. Hernquist, and S. R. Furlanetto, Astrophys. J. **653**, 815 (2006).
[29] J. R. Pritchard and E. Pierpaoli, Phys. Rev. D **78**, 065009 (2008).
[30] C. Gordon and J. R. Pritchard, Phys. Rev. D **80**, 063535 (2009).
[31] P. Adshead, R. Easther, J. Pritchard, and A. Loeb, J. Cosmol. Astropart. Phys. 02 (2011) 021.
[32] J. C. Pober, A. R. Parsons, D. R. DeBoer, P. McDonald, M. McQuinn, J. E. Aguirre, Z. Ali, R. F. Bradley, T.-C. Chang, and M. F. Morales, Astron. J. **145**, 65 (2013).
[33] M. A. Alvarez, E. Komatsu, O. Dore, and P. R. Shapiro, Astrophys. J. **647**, 840 (2006).
[34] P. Adshead and S. Furlanetto, Mon. Not. R. Astron. Soc. **384**, 291 (2008).
[35] T. Giannantonio and R. Crittenden, Mon. Not. R. Astron. Soc. **381**, 819 (2007).
[36] V. Jelić, S. Zaroubi, N. Aghanim, M. Douspis, L. V. E. Koopmans, M. Langer, G. Mellema, H. Tashiro, and R. M. Thomas, Mon. Not. R. Astron. Soc. **402**, 2279 (2010).
[37] H. Tashiro, N. Aghanim, M. Langer, M. Douspis, S. Zaroubi, and V. Jelic, Mon. Not. R. Astron. Soc. **402**, 2617 (2010).
[38] Q. Ma, K. Helgason, E. Komatsu, B. Ciardi, and A. Ferrara, Mon. Not. R. Astron. Soc. **476**, 4025 (2018).
[39] P. La Plante, A. Lidz, J. Aguirre, and S. Kohn, Astrophys. J. **899**, 40 (2020).
[40] C. Dvorkin and K. M. Smith, Phys. Rev. D **79**, 043003 (2009).
[41] S. Furlanetto, M. Zaldarriaga, and L. Hernquist, Astrophys. J. **613**, 1 (2004).
[42] O. Zahn, A. Lidz, M. McQuinn, S. Dutta, L. Hernquist, M. Zaldarriaga, and S. R. Furlanetto, Astrophys. J. **654**, 12 (2007).
[43] M. Zaldarriaga, S. R. Furlanetto, and L. Hernquist, Astrophys. J. **608**, 622 (2004).
[44] X. Wang and W. Hu, Astrophys. J. **643**, 585 (2006).
[45] A. Cooray and R. K. Sheth, Phys. Rep. **372**, 1 (2002).
[46] C. Dvorkin, W. Hu, and K. M. Smith, Phys. Rev. D **79**, 107302 (2009).
[47] P. D. Meerburg, J. Meyers, K. M. Smith, and A. van Engelen, Phys. Rev. D **95**, 123538 (2017).
[48] R. Ansari *et al.* (Cosmic Visions 21 cm), arXiv:1810.09572.
[49] SKA forecast details: We consider.

[50] D. Li, H.-M. Zhu, and U.-L. Pen, Phys. Rev. D **100**, 023517 (2019).
[51] S. Gagnon-Hartman, Y. Cui, A. Liu, and S. Ravanbakhsh, Mon. Not. R. Astron. Soc. **504**, 4716 (2021).
[52] A. Liu, Y. Zhang, and A. R. Parsons, Astrophys. J. **833**, 242 (2016).
[53] S. C. Hotinli, J. B. Mertens, M. C. Johnson, and M. Kamionkowski, Phys. Rev. D **100**, 103528 (2019).
[54] G. Sato-Polito, J. L. Bernal, K. K. Boddy, and M. Kamionkowski, Phys. Rev. D **103**, 083519 (2021).
[55] Z. Pan and M. C. Johnson, Phys. Rev. D **100**, 083522 (2019).
[56] D. Contreras, M. C. Johnson, and J. B. Mertens, J. Cosmol. Astropart. Phys. 10 (2019) 024.
[57] J. I. Cayuso and M. C. Johnson, Phys. Rev. D **101**, 123508 (2020).
[58] M. Münchmeyer, M. S. Madhavacheril, S. Ferraro, M. C. Johnson, and K. M. Smith, Phys. Rev. D **100**, 083508 (2019).
[59] N. Aghanim *et al.* (Planck Collaboration), Astron. Astrophys. **641**, A6 (2020).
[60] R. Braun, A. Bonaldi, T. Bourke, E. Keane, and J. Wagg, arXiv:1912.12699.